Influence of Crystalline Structure of Ceria on the Remaining Particles in the STI CMP

Journal of The Electrochemical Society, **154** (7) H642-H646 (2007)
0013-4651/2007/154(7)/H642/5/$20.00 © The Electrochemical Society

Influence of Crystalline Structure of Ceria on the Remaining Particles in the STI CMP

Sang-Kyun Kim,[a] Ye-Hwan Kim,[a] Ungyu Paik,[a,z] and Jea-Gun Park[b]

[a]*Division of Advanced Materials Science Engineering, and* [b]*Nano-SOI Process Laboratory, Hanyang University, Seoul 133-791, Korea*

The structural characteristics of nanosized ceria particles were investigated to clarify the relationship between the structural characteristics of abrasives and the problem of residual particles in shallow trench isolation chemical mechanical planarization (STI CMP). The ceria particles were synthesized via a solid-state displacement reaction method, and their crystalline structure was controlled by regulating the oxygen partial pressure at the reaction site on the precursor. In a calcination process with a high oxygen concentration, the synthesized ceria particles had a cubic fluorite structure (CeO_2) because of the decarbonation of the cerium precursor at a high oxygen partial pressure. The particles calcined with a low oxygen partial pressure had an included hexagonal structure (Ce_2O_3). The ceria slurry prepared with the cubic CeO_2 yielded a higher removal rate than the slurry prepared with the hexagonal Ce_2O_3. Furthermore, the ceria slurry with the cubic structured particles had less residual particles on the oxide film than the slurry with the hexagonal structured particles. The resulting residual particles originated because Ce_2O_3 is easily agglomerated and adsorbed on the wafer surface due to the high surface activity resulting from the oxygen vacancy on the particle surface.
 [DOI: 10.1149/1.2735923]

Manuscript submitted April 26, 2006; revised manuscript received January 8, 2007. Available electronically May 22, 2007.

In the manufacture of next-generation LSI devices, chemical mechanical planarization (CMP) is a key process used for the planarization of wafer surfaces to achieve a multilevel interconnection.[1-3] A wide range of global planarization is required to attain a sufficient depth of focus (DOF) within the process margin of exposure equipment for the fine process technology patterns. In the CMP process, slurry conditions are critical for the realization of high-quality wafer devices due to the chemical and mechanical interactions with the deposited film surface. The required dimensions of current semiconductor devices are decreasing below 50 nm. Because of this, a ceria-based slurry is widely used instead of other abrasive slurries in shallow trench isolation (STI) as well as interlayer dielectric (ILD) CMP for the manufacture of dynamic random access memory (DRAM) and flash memory devices, due to the good removal selectivity, chip uniformity, global planarity, and the high polishing efficiency of the oxide film.[4] However, the ceria slurry induces defects on the wafer surface because of the large, abrasive agglomerated particles resulting from poor dispersion stability. During CMP, the agglomerated particles easily stick to the wafer surface, which results in residual particles and scratches on the wafer surface.[5-9] In order to reduce the surface defects, particle agglomeration should be prevented by the stabilization of the ceria suspension.[10-12] In general, the dispersion stability can be improved by adding an adequate polymeric dispersant. However, the stabilization of the ceria suspension using a polymeric dispersant has limitations in successfully eliminating the agglomerated particles which can induce scratches on the wafer surface. Therefore, a new method which can prevent the agglomeration of the ceria particle must be proposed. In this study, we considered the intrinsic properties of the particles themselves as a critical factor to prevent agglomeration and adhesion on the wafer, and thus, an attempt to control the intrinsic properties of the ceria powder was made. Ceria powder has been synthesized by many different methods including wet precipitation, sol-gel, hydrothermal, mechanochemical, and solid-state displacement reactions (calcinations).[4,13] The solid-state displacement reaction is widely used for the synthesis of ceria particles because the crystallite size of the particles can be easily controlled by varying the calcination conditions such as temperature, time, and oxygen vapor pressure.[14,15] The removal rate of the oxide film is proportional to the crystallite size of the ceria particles.[15] The large crystallite size of the particles results from a high calcination temperature and easily induces many scratches on the wafer surface. Thus, the synthesis of ceria particles at low temperatures is favorable in the CMP process. During the calcination, the by-product carbon dioxide is present around the precursor powder and this causes diffusion resistance for oxygen at the reaction site.[16] It induces an oxygen vacancy within the ceria crystal lattice, which can result in variations of crystal structure. Therefore, in the low-temperature calcination process, the oxygen concentration in the furnace plays an important role in the synthesis reaction because of the acceleration of the decarbonation of the cerium precursor.

In this study, the crystal structure of the ceria particles was controlled by varying the oxygen concentration. The influence of the crystalline structure of the ceria particles on both particle agglomeration in the slurry and residual particles onto the oxide film after CMP was investigated.

Experimental

High-purity cerium carbonate hydrate [$Ce(CO_3)_3$, Juntai, China] was employed as a starting material for the solid-state displacement reaction of the ceria particles. The precursor was calcined under air at 650°C for 4 h, which resulted in a white-yellowish ceria powder. In order to prepare two different crystal structures, the oxygen concentration was controlled by adjusting the air inflow. The particles of samples A and B were synthesized with air flows of 35 and 5 m^3/h, respectively, and the particles of sample C were synthesized without air flow. The crystallite size of the ceria particles was measured by the X-ray diffraction method (RINT/DMAX-2500, Rigaku, Japan) and calculated using the Debye–Scherer equation. The specific surface areas of the powders were estimated utilizing the Brunauer–Emmett–Teller (BET) method (ASAP 2010, Micromeritics, USA). By using nitrogen gas, the samples were outgassed at 250°C for 2 h prior to each analysis to remove physisorbed species from the powder surface. Each calcined ceria powder underwent a wet-mechanical milling process for several hours to reduce the particle size to the target size (240–260 nm as determined by a conventional light-scattering method) and to disperse the particles in an aqueous medium after mixing the powder with deionized water and a dispersant composed of commercially available anionic acrylic polymers [poly(methyl methacrylate), PMAA]. The solid content of the slurry was controlled to a weight fraction of 5%, and the suspension pH was adjusted to 8.4. After preparing the ceria slurry, two samples were dried to investigate the crystallite size and specific surface area. For each sample, the crystallite size and surface area are listed in Table I.

The diffraction patterns of the particles were also investigated using high-resolution TEM (JEOL2010, Jeol, Japan) to certify the crystalline structure and morphology of the ceria particles. Using the

[z] E-mail: upaik@hanyang.ac.kr

Table I. Sample characteristics.

Sample		Crystallite size (nm)	Surface area (m^2/g)
After calcination	Particle A	26.2	3.2
	Particle B	25.9	10.5
	Particle C	25.7	12.7
After mechanical milling	Particle A	25	3.5
	Particle B	21.5	13.4
	Particle C	20.3	15.4

nanobeam aperture (nanobeam size = 3 nm), the diffraction patterns (spot patterns) of the individual particles were obtained.

To investigate agglomeration in the slurries, we measured the number of large particles over 1 μm per unit volume by using a slurry particle counter (Accusizer 780/FX, PSS/Nicomp, USA). The particle counter is a type of large-particle counting equipment that optically detects single particles and counts the number of particles in the tail of a submicrometer distribution. The accuracy of this particle counter was verified with 1.59 μm diam standard latex particles.

Field evaluation of CMP was done using two kinds of slurries. For the CMP evaluation, an 8 in. wafer CMP tool (6EC, Strasbaugh, USA) was used. The polishing pad was a grooved IC1000/SubaIV (Rodel, USA). The film thickness was measured using a Nanospec 180 (Nano-metrics, CA., USA.) to calculate removal rates. For this experiment, the within-wafer nonuniformity (denoted WIWNU) was defined as the standard deviation of the remaining thickness divided by the average of the remaining thickness after CMP. The residual particles and scratches on the oxide film (high-density-plasma SiO_2) were measured using a Surfscan SP1 (KLA-Tencor, USA). After CMP, the wafers were cleaned using an ammonium hydroxide and hydrogen peroxide mixture (APM) solution ($NH_4OH:H_2O_2:H_2O$ = 1:1:10) at 80°C to eliminate residual particles. The polishing test conditions are shown in Table II.

Results and Discussion

Particle and slurry characteristics.— Figure 1 shows the morphology and primary particle sizes of the ceria particles after mechanical milling. The particle size distributions were found to be noticeably different between samples based on the TEM images. The portion of small-sized particles (<20 nm) in samples B and C was larger than in sample A. The initial crystallite size of all as-calcined samples calculated by the Debye–Scherer equation was about 26 nm. However, the crystallite sizes of the particles after mechanical milling became 25, 21.5, and 20.3 nm for samples A, B, and C, respectively, which leads to a significantly different specific surface area for each particle group. After mechanical milling, the particles in all samples had similar size, ranging from 240 to 260 nm. Therefore, the particles (samples B and C) which were calcined at low oxygen concentration are composed of a large number of small crystallites (20.3 and 21.5 nm), while the particles (sample A) which were calcined at a higher oxygen concentration were composed of relatively larger crystallites (25 nm).

Table II. CMP conditions.

Machine model	Strasbaugh 6EC
Slurry	Ceria slurry
Solid concentration of slurry	1 wt %
Pad	IC1000/Suba IV k-groove
Table speed	70 rpm
Spindle speed	70 rpm
Downforce	4 psi
Back-pressure	0 psi
Time	30 s
Flow rate	100 mL/min

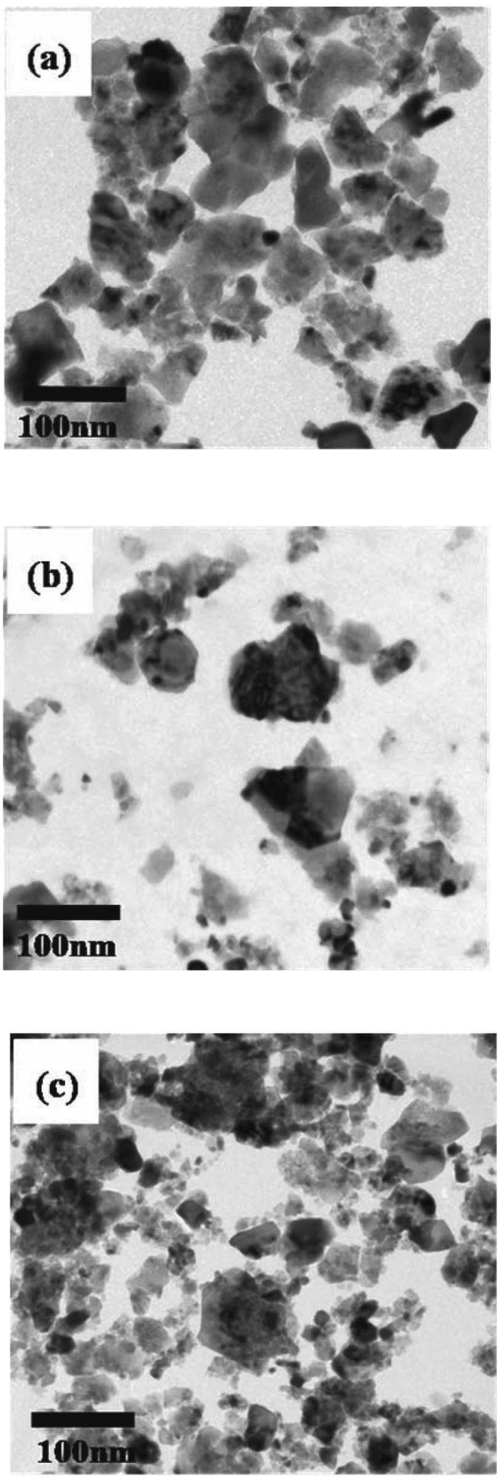

Figure 1. TEM images of the ceria particles: (a) sample A, (b) sample B, and (c) sample C.

With the high-resolution TEM nanobeam diffraction pattern, the crystalline structures of the ceria particles were investigated. The nanobeam diffraction patterns of the particles (Fig. 2) indicate that for sample A, all particles had the cubic fluorite phase of cerium

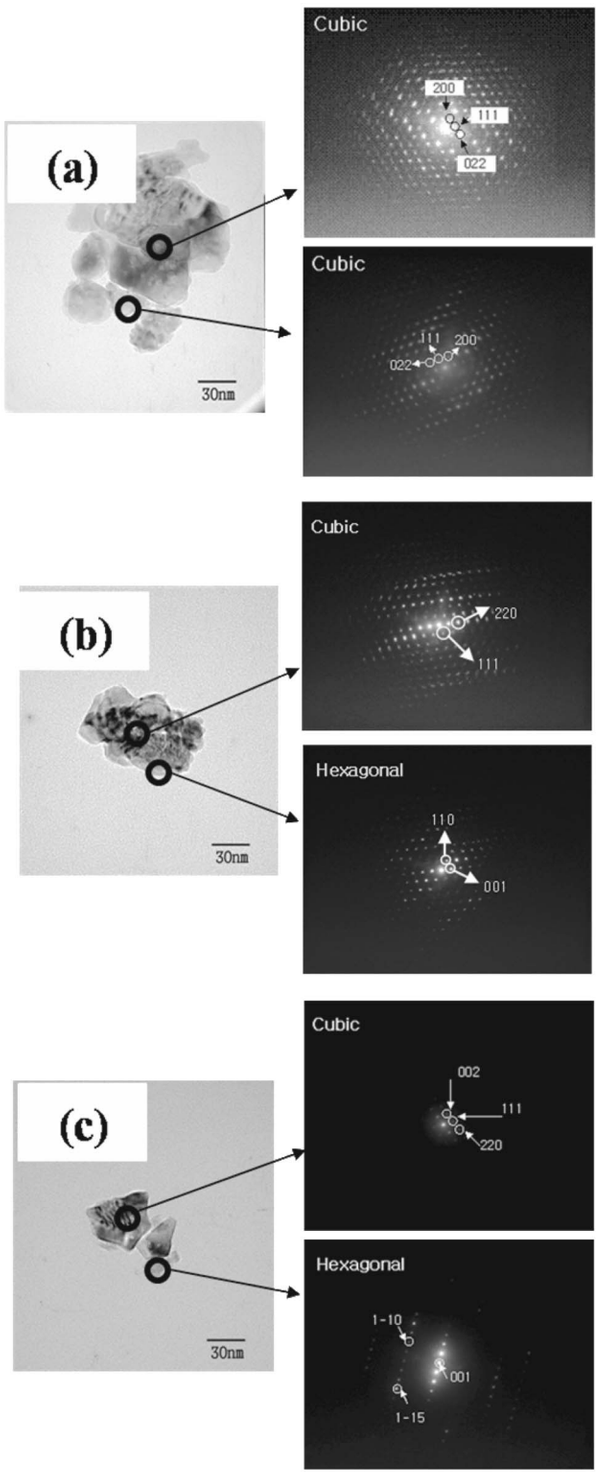

Figure 2. Nanobeam diffraction patterns of the ceria particles: (a) sample A, (b) sample B, and (c) sample C.

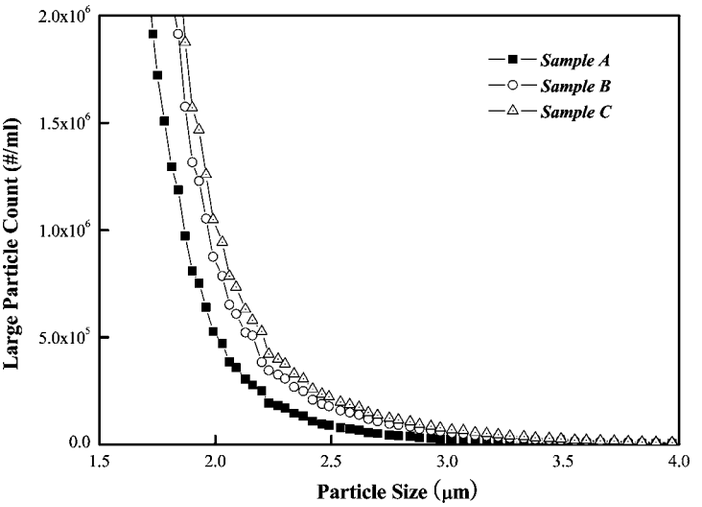

Figure 3. Size of the ceria particles and comparison of large particle counts.

oxide, while samples B and C, which were calcined at a low oxygen concentration, included hexagonally structured particles, especially in the smaller particles. The calcination process from cerium carbonate to cerium oxide consists of a five-step mechanism and includes the mass-transfer of the reacting agent (oxygen) from the bulk atmosphere to the periphery of carbonate, its diffusion through the pore channels of the carbonate, adsorption, reaction with the cerium carbonate, and the desorption of the reaction by-product (carbon dioxide).[16] In this reaction mechanism, several factors influence the physical properties of the synthesized particles during the calcination process. According to previous reports, a low oxygen concentration results in a hexagonal phase cerium oxide rather than the cubic phase due to the insufficient oxidation of Ce^{3+} to Ce^{4+}.[17] In the absence of an external oxygen supply, the hexagonal CeO_x phase is reported to be observed between 400 and 500°C and the oxidation of CeO_x is complete above 800°C, which results in the transformation from hexagonal Ce_2O_3 to cubic CeO_2.[18] Therefore, the hexagonal phase (Ce_2O_3) in samples B and C was formed due to the insufficient oxidation of Ce^{3+} to Ce^{4+}, while the cubic phase (CeO_2) in sample A was obtained due to sufficient oxygen supply.

To investigate agglomeration in the slurries, we measured the number of large particles (>1 μm) per unit volume by using a slurry particle counter and the results are shown in Fig. 3. Samples B and C with a hexagonal crystalline structure have more larger agglomerated particles than sample A. Because the Ce^{3+} and oxygen vacancies in the surface of the hexagonal ceria particle are linked to anionic vacancies with hydroxyl groups, chemisorption and agglomeration easily occurred with the neighboring cation-species and bared ceria surface.[18,19] Moreover, samples B and C have many small particles, which were confirmed to have a mainly hexagonal crystalline structure (Fig. 3). The van der Waals attractive force is well known to increase with decreasing particle size; therefore, the large agglomerated particles in samples B and C are attributed to the presence of small-sized particles.

CMP performance.— CMP was performed with the ceria slurry which was prepared by adding an adequate amount of commercially available anionic acrylic polymers (PMAA). Cubic CeO_2 (sample A) and CeO_2 with included hexagonal Ce_2O_3 particles (sample C) were used as abrasive particles. The removal rate trends along the radius and WIWNU of the oxide film are shown in Fig. 4. In Fig. 4a, there is a remarkable difference between the oxide film removal rates of samples A and C. The removal rate of the oxide film was dependent on the crystallinity of the ceria particles.[15] The polishing of the oxide film was mainly affected by the chemical interaction between the ceria particles and the oxide (SiO_2) film, which reacted with the hydrated surface to form covalent bonds such as Ce–O–Si and then pulled off the oxide lumps.[20,21] As shown in Fig. 1, the particles of sample A had a larger crystallinity and narrower particle size distribution than those of sample C. Because the hexagonal structured ceria particles and the agglomerated particles of sample C were

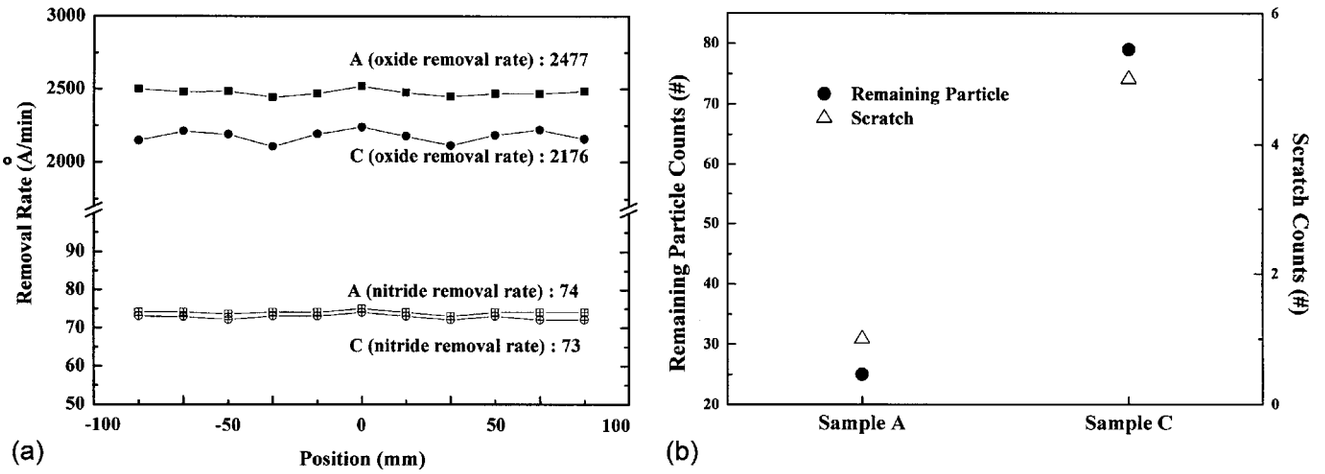

Figure 4. The result of the CMP field evaluation: (a) average removal rate and (b) the WIWNU of oxide wafer.

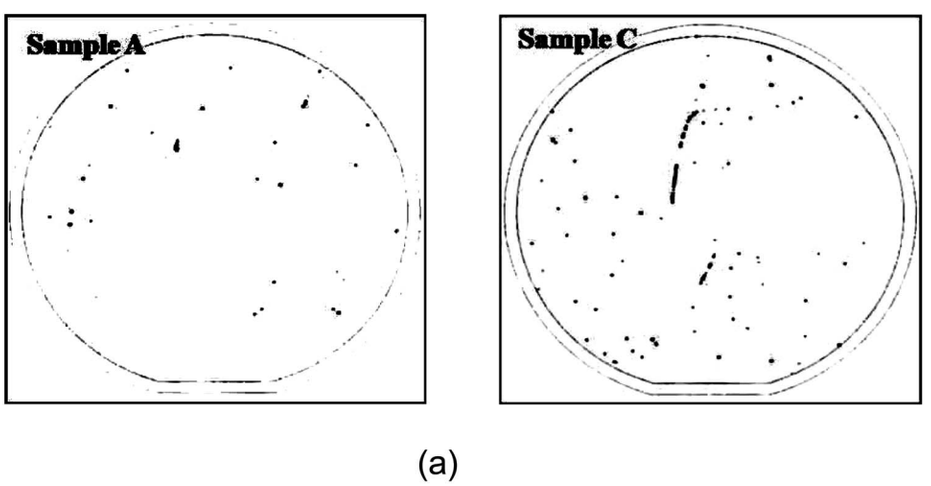

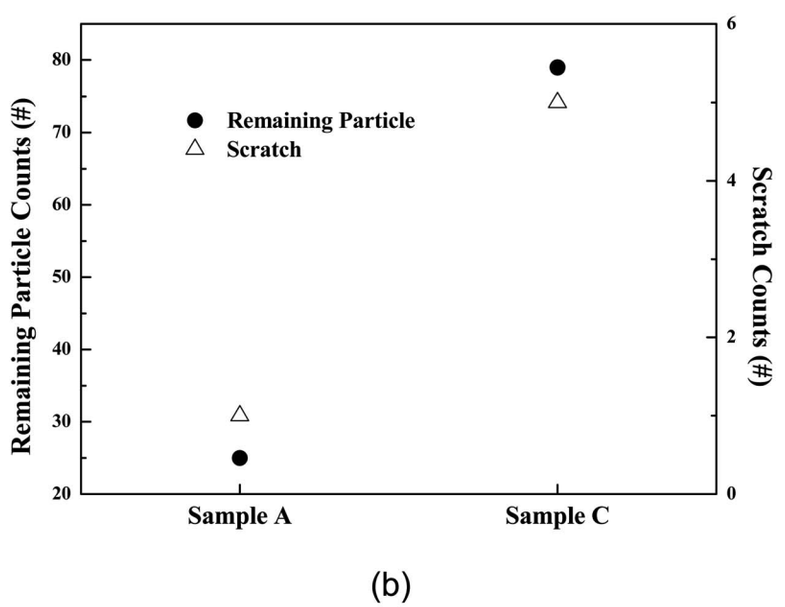

Figure 5. Remaining particle maps on the oxide film measured with the Sufscan 7700.

easily broken apart during the CMP process, these particles did not penetrate the viscous layer on the oxide film.[22] Thus, the removal rate of sample C was low, resulting in poor oxide due to nitride selectivity. The surface of the silicon nitride film during polishing was passivated with an adsorptive surfactant in the slurry, which prevents the abrasive from directly contacting the film surface.[23,24] Hence, the removal rates for the Si_3N_4 film were not influenced by the crystalline structure of the ceria particles. In addition, the slurry with agglomerated particles was hardly propagated over the whole wafer surface due to poor stability. Thus, as shown in Fig. 4b, sample C has a higher WIWNU and a lower removal rate of wafer edge position than those of sample A.

During the CMP, the agglomerated particles were easily stuck to the wafer surface by the small interactive force between the abrasive and oxide film. In particular, it is these sticking particles that induce the surface scratches on the wafer due to the compressive and shear forces between the wafer and pad. Therefore, agglomerated particles are a major cause for the residual particles and the microscratches in the CMP process. The maps of the residual particle counts and scratch counts are shown in Fig. 5a and b, respectively. The smaller particles observed in sample C had a high surface activity and specific surface area. As shown in Fig. 5a, the residual particle counts of sample C are much larger than that of sample A. These residual particles induced the surface scratching during the CMP process. In Fig. 5b, the scratch counts of sample C are also larger than sample A. Consequently, the ceria powders that include hexagonal structured particles were easily broken down into the smaller particles and induced particle adhesion on the wafer surface. Therefore, the ceria particles should be calcined to a cubic structure through control of the oxygen concentration.

Conclusions

We have investigated the effects of the crystalline structure of nanosized ceria particles on the physicochemical properties of the ceria slurry and the residual particles and microscratches during STI CMP. The crystalline structures of the particles were remarkably different as a function of air inflow conditions. The particles calcined at a higher oxygen concentration were of a cubic structure (CeO_2) but the particles calcined at a low oxygen concentration included the hexagonal structure (Ce_2O_3). The hexagonal structured particles had a smaller particle size than the cubic structured particles. These smaller particles had a high surface area, which resulted in large attractive forces between particles. This caused a low removal rate, high numbers of residual particles, and surface scratches during STI CMP. Consequently, we concluded that the differences in the crystalline structure of the ceria particles had a profound effect on the dispersion stability and the residual particles after STI CMP.

Acknowledgement

This work was financially supported by Korea Institute of Science and Technology Evaluation and Planning (KISTEP) through the National Research Laboratory (NRL) program.

Hanyang University assisted in meeting the publication costs of this article.

References

1. S. Wolfe, *Silicon Processing*, Vol. 4, Chap. 8, p. 313, Lattice Press, Sunset Beach, CA (2002).
2. C. F. Lin, W. T. Tseng, and M. S. Feng, *J. Electrochem. Soc.*, **146**, 1984 (1999).
3. S. Sivaram, H. Bath, R. Leggeti, A. Maury, K. Monnig, and R. Tolles, *Solid State Technol.*, **35-5**, 87 (1992).
4. J. H. So, D. J. Lee, Y.-J. Cho, M.-H, Ahn, I.-Y. Lee, S.-J. Jeon, S. Kim, and S.-M. Yang, in *Proceedings of the Korean CMP-UGM Conference*, The Korean Institute of Electrical and Electronic Material Engineers, Paper 2 (2005).
5. T. Detzel, S. Hosali, A. Sethuraman, J. F. Wang, and L. Cook, in *Proceedings of the CMP-MIC Conference*, Institute for Microelectronics Inter-Connection, p. 202 (1997).
6. G. B. Basim, J. J. Adler, U. Mahajan, R. K. Singh, and B. M. Moudgil, *J. Electrochem. Soc.*, **147**, 3523 (2000).
7. R. K. Singh, S. M. Lee, K. S. Choi, G. B. Basim, W. Choi., Z. Chen, and B. M. Moudgil, *Mater. Res. Bull.*, **2002**, 752 (Oct).
8. T. L. Neo, E. S. Y. Shang, and C. M. Chong, in *Proceedings of the International Symposium on Semiconductor Manufacturing*, IEEE, p. 321 (2001).
9. Y. J. Seo, G. U. Kim, and W. S. Lee, *Microelectron. Eng.*, **71**, 209 (2004).
10. B. V. Velamakanni, J. C. Chang, F. F. Lange, and D. S. Pearson, *Langmuir*, **6**, 1323 (1990).
11. J. C. Chang, B. V. Velamakanni, F. F. Lange, and D. S. Pearson, *J. Am. Ceram. Soc.*, **74**, 291 (1991).
12. L. Bergstrom, K. Shinozaki, H. Tomiyama, and N. Mizutani, *J. Am. Ceram. Soc.*, **80**, 833 (1997).
13. S. K. Tadokoro and E. N. S. Muccillo, *J. Eur. Ceram. Soc.*, **22**, 1723 (2002).
14. S. K. Kim, U. Paik, S. G. Oh, Y. K. Park, T. Katoh, and J. G. Park, *Jpn. J. Appl. Phys., Part 1*, **42**, 1227 (2003).
15. S. K. Kim, P. W. Yoon, U. Paik, T. Katoh, and J. G. Park, *Jpn. J. Appl. Phys., Part 1*, **43**, 7427 (2004).
16. O. Levenspiel, *Chemical Reaction Engineering*, 3rd ed., Chap. 18, p. 378, Wiley, New York (1999).
17. F. Sadi, D. Duprez, F. Gérard, and A. Miloudi, *J. Catal.*, **213**, 226 (2003).
18. D. Terribile, J. Llorca, M. Boaro, C. de Leitenburg, G. Dolcetti, and A. Trovarelli, *Electrochem. Commun.*, **17**, 1897 (1998).
19. S. Tsunekawa, R. Sivamohan, S. Ito, A. Kasuya, and T. Fukuda, *Nanostruct. Mater.*, **11**(1), 141 (1999).
20. K. Hirai, H. Ohtsuki, T. Ashizawa, and Y. Kurata, Hitachi Chemical Tech., Report No. 35, 17 (2000).
21. Y. Homma, T. Furusawa, H. Morishima, and H. Sato, *Solid-State Electron.*, **41**, 1005 (1997).
22. H. G. Kang, T. Katoh, M. Y. Lee, H. S. Park, U. Paik, and J. G. Park, *Jpn. J. Appl. Phys., Part 1*, **43**, 1060 (2004).
23. J. G. Park, T. Katoh, W. M. Lee, H. Jeon, and U. Paik, *Jpn. J. Appl. Phys., Part 1*, **42**, 5420 (2003).
24. S. K. Kim, S. K. Lee, U. Paik, and T. Katoh, *J. Mater. Res.*, **18**, 2163 (2003).